Mon. Not. R. Astron. Soc. **000**, 1–9 (2011) Printed 18 October 2014 (MN LaTeX style file v2.2)

Investigations of the emission geometry of the four-component radio pulsar J0631+1036

Mateus M. Teixeira[1], Joanna M. Rankin[1,3], Geoffrey A.E. Wright[2,3] & J. Dyks[4]
[1] *Department of Physics, University of Vermont, Burlington, VT 05405*⋆
[2] *Astronomy Centre, University of Sussex, Falmer, BN1 9QJ, UK*†
[3] *Astronomical Institute "Anton Pannekoek", University of Amsterdam, Science Park 904, 1098 XH Amsterdam, The Netherlands*
[4] *Nicolaus Copernicus Astronomical Center, Rabiańska 8, 87-100, Toruń, Poland*‡

Originally drafted 2011 09 22

ABSTRACT
Radio pulsar J0631+1036 presents a remarkably clear example of a rare four-component profile, and with apparently large aberration/retardation indicated by its linear polarization-angle traverse, but on closer study its profiles are difficult to understand and interpret. Given the broad success of the core/double-cone geometric model in describing the profiles of slower pulsars, we assess whether it could be appropriate for J0631+1036. The emission geometry resulting from application of this model is difficult to reconcile with the well resolved forms of the inner component pair. It is shown that the profile properties can be better explained if our line of sight intersects four lobes of a nearly symmetric beam which is azimuthally-structured about the pulsar's dipole axis. This model would suggest that the dipole field is highly inclined to the rotation axis and viewed at a large impact angle, a geometry consistent with recent high-energy observations.

Key words: miscellaneous – aberration/retardation – emission height – emission geometry – methods: – data analysis – pulsars: general, individual (J0631+1036)

I. INTRODUCTION

The very unusual pulse profile of pulsar J0631+1036 in Figure 1 (top) consists of two pairs of nearly symmetrical components, all highly linearly polarized at higher frequencies. Four-component forms are rare in the radio pulsar population, whereas one finds hundreds of triple and scores of five-component profiles. For slower pulsars (rotation periods greater than 100 ms or so), the core-double cone beaming model provides a successful quantitative description for the vast majority of stars (*e.g.,* "Empirical Theory" series VI, Rankin 1993; ET IX, Mitra & Rankin 2010). Triple profiles then usually represent sightline traverses through one cone and the core, whereas five-component profiles reflect both cones and the core. The few known four-component profiles exhibit forms similar to those of five-component pulsars—but absent a central core feature owing either to weakness or to a sightline that just misses it (*e.g.,* B1738–08 in ET VI)—either case resulting in significant emission at the profile center. Also the inner conal component pair is generally weaker with a flatter spectrum. Thus these four components do not appear evenly spaced—but rather as clear leading and trailing pairs. The J0631+1036 21-cm profile is thus striking on all these grounds: the near even spacing of its four components; the deep emission minimum at the center; and the relative weakness of its outer component pair.

This is not all: the fractional linear polarization of the high frequency profiles in Fig. 1 is unusually complete across almost their full widths. Most radio pulsar profiles have substantial linear polarization, but nearly complete polarization is rare. Further, the accompanying polarization position-angle (hereafter PPA) traverse of J0631+1036 is no less remarkable, sweeping the greater part of the canonical 180° associated with a central sightline geometry, but in a strikingly asymmetric manner. Indeed, the steepest gradient point falls not near the profile center but on its far trailing edge, clearly suggesting that aberration/retardation (hereafter A/R) is a significant factor in its structure.

PSR J0631+1036 was discovered by Zepka *et al.* (1996), in the course of an Arecibo search targeted at *Einstein* IPC X-ray sources. It has a rotation period P

⋆ Mateus.Teixeira@uvm.edu; Joanna.Rankin@uvm.edu
† G.Wright@sussex.ac.uk
‡ jinx@ncac.torun.pl

© 2011 RAS

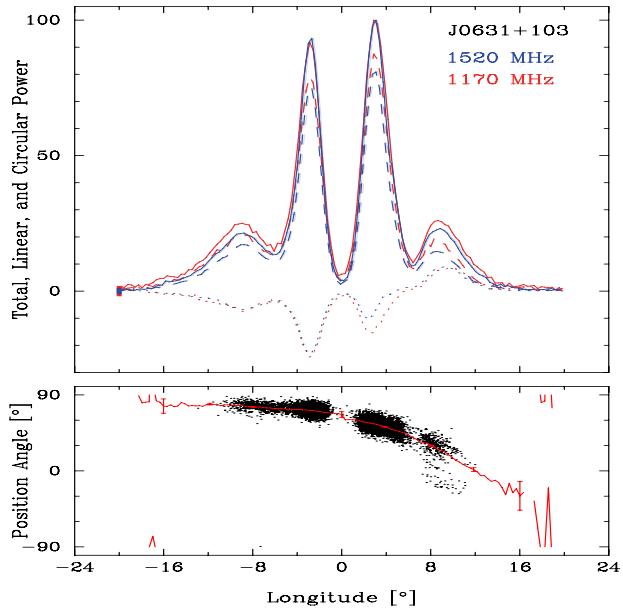

Figure 1. Overlaid average profiles at 1170 MHz (red) and 1520 MHz (blue), including polarimetry information (Stokes I, solid curve; linear $[\sqrt{Q^2+U^2}]$ dashed; and circular V dotted), for pulsar J0631+1036 on MJD 54540 **scaled to an arbitrary intensity maximum**. The average PPA $[=\frac{1}{2}\tan^{-1}U/Q]$ traverse in the bottom panel corresponds to that of the three combined bands. The error box at the left of the figure shows the resolution as well as three standard deviations in the off-pulse noise level.

of 0.288 s and a spindown of 1.05x10^{-13} s/s, giving it a large magnetic field (5.6x10^{12} G), acceleration potential across the polar cap (67x10^{12} V) and rotational energy loss rate (1.7x10^{35} erg/s). The pulsar was also detected at γ-ray energies by the Fermi-LAT Observatory (Weltevrede *et al.* 2010), and Seyffert *et al.* (2011) further discuss its interpretation. Such a high energy-loss rate (indeed, high energy detection!) and acceleration potential suggests that its emission might well be core dominated, but nothing about its profile form seems to support this interpretation. See Zepka *et al.*'s fig. 3, where the pulsar's profile in four bands between 430 and 2380 MHz is plotted.

Finally, the pulsar's evolution with frequency is also difficult to understand. At 430 MHz in the above Zepka *et al.* figure, the J0631+1036 profile is much broader and has the form of an unresolved double. Such a profile evolution—that is, broader at longer wavelengths—is an expected aspect of outer conal emission; however, that the emission component number appears to change from one frequency to another—this is virtually unknown and deserves explanation.

This pulsar has unusually high dispersion (DM) and rotation (RM) measures for its position near the Galactic anticenter—suggesting a distance of 6.5 kpc, whereas its actual distance is probably around 1 kpc—and Zepka *et al.* (1996) speculate that it may be interacting with a relatively dense environment which is not its SNR of birth. The star also experiences an exceptionally frequent number of glitches, often of a non-standard character (Espinoza *et al.* 2011). Might these unusual features somehow be linked to J0631+1036's unusual profile?

Table 1. Arecibo Polarimetry Observations

Band	MJD Date	BW/chans (MHz)	Resolution (°)	Length (mins)
P	54016 2006 Oct 8	25/256	2.81	20
L	54540 2008 Mar 15	300/384	0.32	20
L	56500	258/384	0.70	10
U	2013 Jul 27	12/128	0.70	60
P		50/2048	1.41	60
L	56514	258/384	1.25	6.2
U	2013 Aug 10	22.7/1024	1.41	60
P		50/4096	1.41	47.3

Observations with center frequencies of 327 MHz (P), 430 MHz (U) and 1170, 1420 and 1520 MHz (L) were carried out with the Wideband Arecibo Pulsar Processor before MJD 56000 [see Smith *et al.* (2013) for observational details] and the Mock Spectrometers thereafter (*e.g.,* Mitra *et al.* 2014). Four bands of 86 (12.5) MHz centered at 1270, 1420, 1520 and 1620 MHz (308.25, 320.75, 333.25, 345.75) were used to cover the available L (P) receiver bands.

In preparing this report we have drawn on some new Arecibo observations as well as soliciting a range of theoretical opinions in an effort to understand and explain pulsar J0631+1036's multifrequency profiles. §II then presents the new observations and their geometric analyses. §III discusses the implications of this geometry theoretically. §§IV-VI present different possible emission models, and §VII provides and overall summary and discussion.

II. DOUBLE CONE/CORE BEAM MODEL

Morphology & Conal Spreading

The average profile of pulsar J0631+1036 develops remarkably over the three octaves of available observations, but the Zepka *et al.* profiles leave important questions unresolved: Their meter-wavelength (430-MHz) total power profile seems to exhibit a resolved conal double (D) configuration [as per the classification in Rankin 1983 (ET I) & ET VI]; however, it is also less well resolved than the others, and scattering may be an issue. Further, the profiles appear to be time aligned, but the paper does not explicitly say so, and there is no low frequency polarimetry.

In order to resolve these issues we carried out Arecibo polarimetry observations at three bands in close succession on the same days as indicated in Table 1. Two profiles from the MJD 56514 observation are shown in Figure 2 **and are aligned using a DM value of 125.36 pc cm^{-3}** (Weltevrede *et al.* 2010) and the (Yuan *et al.* 2010) timing solution. The 430-MHz profile (bottom panel) is better resolved than the Zepka *et al.* one and shows clear four-fold structure corresponding to the four components at 1.4 GHz (top panel). The 327-MHz

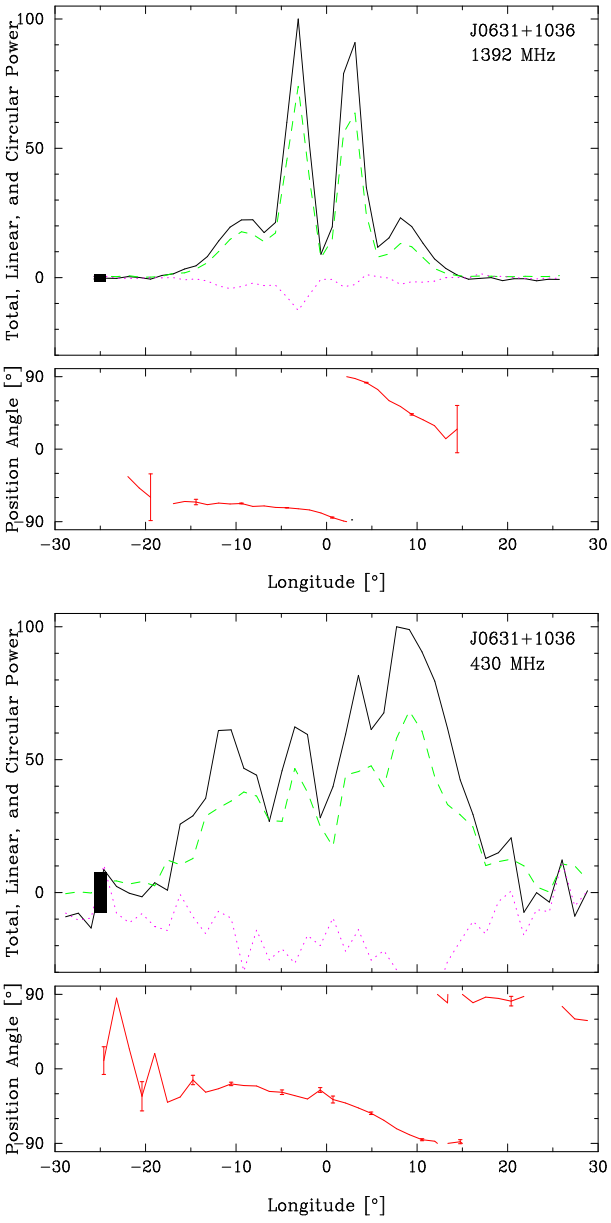

Figure 2. Time-aligned profiles corresponding to two of the three frequency bands observed on MJD 56514: 1392 MHz (top) and 430 MHz (bottom) after Fig. 1. The four components of the star's profile show clearly in this 430-MHz profile. Note also that while the latter is much broader overall than at 1.4 GHz, the component peaks fall at very similar spacings—the inner cone spacing hardly altered and that of the outer conal components only 2–4° wider.

profile (not shown), however, has only an unresolved double structure similar to that in the Zepka profile. Figure 3 shows another 327-MHz profile from MJD 54016, where the four components also are conflated into a unresolved double form. Note, however, the increased breadth, depolarization and flattening of the PPA traverse on the trailing edge (at 430 MHz as well)—suggesting that the above authors were correct in attributing the low frequency broadening to scattering.

This said, we have found the star's low frequency profiles somewhat variable from day to day. The four

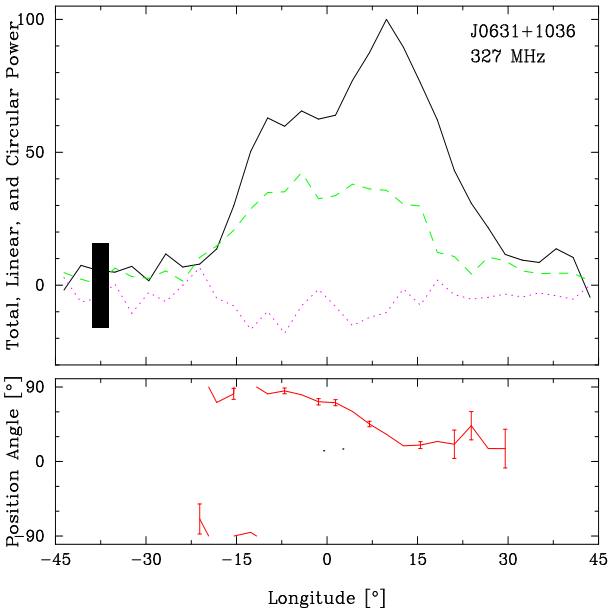

Figure 3. Polarized profile at 327-MHz from MJD 54016 after Fig. 1. Note the highly linearly polarized leading and depolarized trailing edges and the flattened trailing PPA traverse.

components in the 430-MHz profile of Fig. 2 are well resolved; however a very similar observation two weeks earlier showed a profile much like that of Zepka *et al.*'s. Similarly, the unshown 327-MHz profile corresponding to those in Fig. 2 showed only moderate linear polarization which was uniform across the profile, whereas other 327-MHz observations show a more highly polarized leading region and a depolarized trailing one as in Fig. 3.

These profiles then resolve the mysteries about J0631+1036's profile evolution: the outer conal component pair strengthens relative to the inner one with wavelength, so that at meter wavelengths both pairs have comparable intensities—a trend that was discernible even in Fig. 1 and the Zepka *et al.* profiles; and the four-fold structure at 327-MHz (and perhaps sometimes at 430 MHz) is conflated by scattering.

The full width at half maximum (FWHM) width for the 1520-MHz total power profile—**here following the procedures of ET VI in using the outside half power points of the putative outer conal component pair**—is some ∼22.5°, significantly narrower than the ∼34° FWHM of the 327-MHz profile, as would be expected for an outer conal emission geometry. By using our other profiles **similarly** at 1170 and 1420 MHz and those of Zepka *et al.* at 430, 1665 and 2380 MHz (23.2, 22.0, 31, 21.5 and 21°, respectively) we were able to assemble the information for modeling in Table 2, where we see that the values exhibit the expected increase with wavelength.

FWHM values for the inner component pair, by contrast, change little with frequency as is expected for an inner cone, hovering around 8.3° and to perhaps 9° at 430 MHz. Moreover, the inner-conal component pair weakens with wavelength relative to the outer pair, again a typical behavior in double cone profiles.

Figure 1 exhibits the star's dramatic high frequency

Table 2. Double Cone Geometry Model for PSR J0631+1036.

Freq (MHz)	w_i (°)	ρ_i (°)	w_o (°)	ρ_o (°)	β/ρ_o	h_i (km)	h_o (km)
2380	8.3	7.3	21.0	10.3	–0.65	103	204
1665	8.3	7.3	21.5	10.4	–0.64	103	209
1520	8.3	7.3	22.0	10.6	–0.63	103	215
1420	8.3	7.3	22.5	10.7	–0.62	103	221
1170	8.3	7.3	23.2	10.9	–0.61	103	230
430	9	7.5	31	13.4	–0.50	107	343
327	—	—	34	14.4	–0.46	—	395

Note: w_i **and** w_o **are the outside half-power widths of the putative inner and outer cones, respectively, as are** ρ_i**,** ρ_o **and** h_i**,** h_o **the corresponding beam radii and characteristic emission heights per the conventions of ET VI.** α is taken as 52° and β as –6.7°, such that R_{PA} [$=\sin\alpha/\sin\beta$] is –6.8°/°. The β/ρ_i column is omitted because its value never departs from –0.9.

PPA traverse. In these profiles, we see a well resolved set of four highly polarized and symmetrical components, with near zero emission between the inner pair. The PPA swings through more than 100° with the inflection point falling under the trailing component. Note that a very similar but less complete traverse is seen in Fig. 3—though its depolarized and flattened trailing region appears to reflect the effects of scattering.

A single-vector-model (hereafter SVM) fit to the pulsar's PPA traverse at 1520 MHz was computed. The four-parameter fit confirms that the steepest gradient (SG) point of the traverse falls at +9.7°. It also determines nominal values of the magnetic colatitude α and sightline impact angle β. However, these latter values are typically 99% correlated, so it is the PPA slope R_{PA} [$=\sin\alpha/\sin\beta$] at the SG point that is significant and well determined (see also ET IX). This value is –6.8±0.2°/°.

A/R Emission-Height Estimation

As we saw in the J0631+1036 profiles above, the star's PPA traverse is so SVM-like and its SG point so dramatically delayed with respect to the profile center that the situation seems almost to scream out for A/R analysis. Not so fast, however! The physical basis and practical application of A/R analysis was first developed by Blaskiewicz *et al.* (1991; hereafter BCW), but only over the last decade or so has it found wide application and provided increasingly consistent results. Fundamental to all A/R analyses is reliable determination of a profile center which can be interpreted as the longitude of the magnetic axis. Such interpretations have followed one of two courses: a) taking the midpoint between two conal components relative to the PPA SG point as falling symmetrically on either side of the magnetic axis longitude (BCW), or b) taking the center of a core component as marking the magnetic axis longitude [Malov & Suleymanova (1998) and later Gangadhara & Gupta (2001), hereafter G&G].

Pulsar J0631+1036's unusual profile above, however, gives us pause. While we do see evidence that the star's four components represent inner and outer conal component pairs, we do not want to rush to this conclusion. However, their striking symmetry remains—as well as the striking asymmetry of the PPA traverse—and it is very hard to understand how the longitude of the magnetic axis could fall at any other point than midway between the centers of the two conal component pairs and the PPA SG point.

Table 3. Aberration/retardation results for PSR J0631+1036.

ϕ_l (°)	ϕ_t (°)	ν (°)	ρ (°)	r_{em} (km)	s_L
Outer cone					
–20.8	+1.3	–9.8	10.6	585	0.60
(0.2)	(0.2)	(0.14)	(0.1)	(8)	(0.01)
Inner cone					
–13.6	–5.4	–9.5	7.4	570	0.42
(0.1)	(0.1)	(0.07)	(0.03)	(4)	(0.01)

Note: ϕ_l **and** ϕ_t **are the respective leading and trailing component positions and** ν **their difference.** ρ **is the conal radius,** r_{em} **the A/R-estimated physical height and** s_L **the fractional annulus on the polar cap.** The A/R height values do not depend on the emission geometry, but computation of the conal and "footprint" radii do. The α and β values are taken as in Table 2.

So emboldened, we have conducted an A/R analysis of the former type. However, in terms of computations, all are the same, and the values in Table 3 are similar to tables in previous such efforts in G&G, Srostlik & Rankin (2005), Force & Rankin (2010) or ET IX and are corrected as advised by Dyks *et al.* (2004). ϕ_l^i and ϕ_t^i are the respective leading and trailing longitudes of the centers of one or the other component pairs; ν^i is the computed center of the pair; ρ^i is the computed radius of the emission cone; and r_{em}^i and s_L^i give the physical emission height and relative polar cap annulus, respectively.

The Table 3 results are interesting but strange. The computed physical emission heights of some 600 km for the putative inner and outer cones are indistinguishable within their errors. Physical heights in the 450-600 km range at 1 GHz are expected for outer cones (2-3 times the *characteristic* heights in Table 2 below), but those of inner cones are usually substantially less. Moreover, the emission annuli traced down to the polar cap seem both too close to one another and too well determined.

Quantitative Geometry

The most accurate and consistent estimates of a radio pulsar's emission geometry—that is, its magnetic colatitude α and sightline impact angle β—result from using *both* the angular width information of its profile and the sightline-path information in its PPA traverse. This was the method used in ET VI (Rankin 1993) wherein the bulk of the population with then well measured polarization profiles were found to exhibit a core and double-cone structure—that is, with a half-power core

width of $2.45^\circ P^{-1/2}$ and outside half-power conal radii of $4.3^\circ P^{-1/2}$ and $5.8^\circ P^{-1/2}$ (all at 1 GHz), respectively.[1] And these conal radii then imply *characteristic* emission heights of some 130 and 220 km, respectively.[2]

Pulsar J0631+1036's profile had seemed so unusual that we were slow to assess whether it might represent an inner and outer conal component pair. However, as we have seen in the foregoing sections, the actual properties of this profile—its frequency evolution and PPA traverse—in fact largely appear compatible with this interpretation. What remains then is to ask whether such a geometry is consistent quantitatively. No core feature is discernible at any frequency for this pulsar, so we have no independent means of estimating the pulsar's magnetic colatitude. However, we can ask whether there is any value of α such that the two putative emission cones have their expected dimensions.

Table 2 gives such a double-cone geometric model for J0631+1036. The model values of α and β are taken as 52° and –6.7°, such that the PPA sweep rate R_{PA} is –6.8°/° as determined by the above PPA fit. The respective inner and outer conal radii are computed according to ET VI eq. (4) and the emission heights per eq. (6). Only for this last computation is the pulsar's rotation period P_1 (0.288 s) used to estimate the angular size of the star's polar cap so that magnetic-polar colatitudes can be related to *characteristic* emission heights.

More or less reasonable conal dimensions and characteristic heights are obtained using the model in Table 2 for α values between about 50 and 60°. For α near the upper value, the inner cone exhibits its expected radius and height, and for the lower value the outer cone assumes a radius such that the model 1-GHz *characteristic* emission height is about the expected 220 km. The table is computed for an α of 52°. The lack of simultaneously appropriate conal dimensions for a single α value is unusual, but otherwise the model is not unsatisfactory.

As a whole then, the profile morphology of J0631+1036 suggests that it is a member of the conal quadruple (c**Q**) class (ET VI). Moreover, if the above geometry is correct, there are at least two reasons why no core component is seen in the profile: a) the radius of the core component would be some 2.3°, whereas β is some –6.7°, so the bivariate-Gaussian-shaped core-beam power would be attenuated by a factor of about 20; b) what power remains would appear not in the empty profile region between the two inner conal components, but rather halfway between this point and the PPA SG point, at some +4.8° longitude in Fig. 1, where it would be conflated with power from the trailing inner conal component. This said, the model shows that β/ρ_i is –0.9 for the inner cone, and it is very hard to understand how the two inner conal components could be so narrow and well resolved in this configuration—a matter that is explored further below.

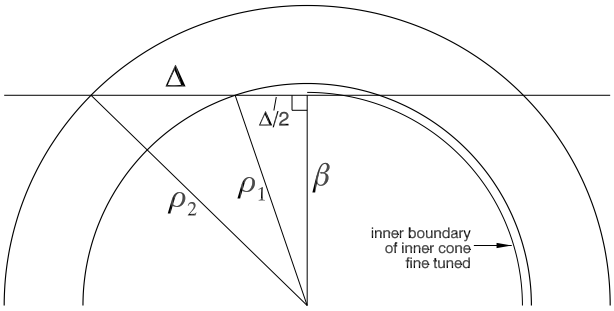

Figure 4. Viewing geometry for a profile with four equidistant components. The horizontal line is the path of a sightline cutting through a beam consisting of two coaxial cones with the size ratio of $\kappa = \rho_1/\rho_2$. The impact angle β and the separation of components Δ are marked. Note the fine tuning required to obtain the equidistance, and the extremely small thickness of the inner side of the inner cone, required to observe the low-flux central minimum.

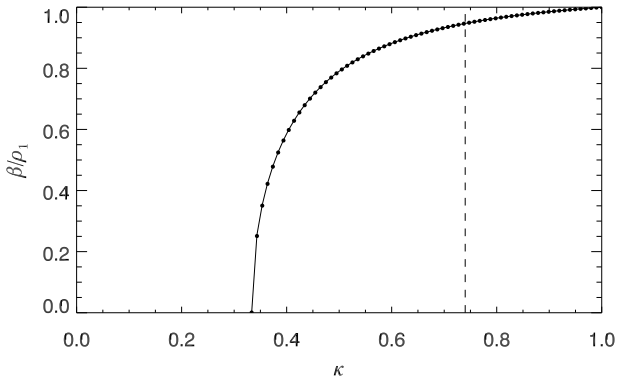

Figure 5. The value of β/ρ_1 as a function of the cone size ratio κ for profiles with equidistant components. The curved line represents the flat solution (eq. 2). The dots present the numerical solution for spherical case. The dashed vertical marks the frequently observed value of κ (Wright 2003). This case is illustrated in the previous figure.

III. GEOMETRY OF NESTED CONES WITH EQUIDISTANT COMPONENTS

In this section we further demonstrate, on purely geometric grounds, that the nested-cone structure inferred for this pulsar is highly unnatural: the near-zero flux at the centre and the nearly equal distances between components ($\Delta \approx 6^\circ$) require fine-tuned geometry with a strange ratio of cone radii and an extremely thin inner cone.

[1] Lyne & Manchester (1988) carried out a similar geometric study and came to many similar conclusions. They also identified a group of some 50 so-called 'partial cone' pulsars that appeared not to exhibit core/conal structure. Reinvestigation of this population using new observations, however, has shown that the vast majority exhibit a core/double-cone profile structure with the above dimensions (ET IX).

[2] Such *characteristic* emission heights are not to be confused with actual, physical emission heights. In the ET VI context, computation of emission heights entails association of the conal emission outer boundary (for both inner and outer cones!) with the "last open" field line. Clearly this is an implausible circumstance physically; its use, however, provides a consistent outer boundary for emission along the edges of the polar flux tube.

This can be proved by considering the flat geometry shown in Fig. 4. The two semicircles represent the maxima of emission cones. Our line of sight crosses them along the horizontal line. The ratio of the angular radii of the two cones is $\kappa = \rho_1/\rho_2$ (shown here as 0.74), and Δ is the separation between the peaks in the profile. Two Pythagorean theorems can be written for the two right-angled triangles: $(\rho_1, \Delta/2, \beta)$ and $(\rho_2, 3\Delta/2, \beta)$, and solved for Δ and β:

$$\frac{|\Delta|}{\rho_1} = \left(\frac{1-\kappa^2}{2\kappa^2}\right)^{1/2}, \quad (1)$$

$$\frac{|\beta|}{\rho_1} = \left(\frac{9\kappa^2-1}{8\kappa^2}\right)^{1/2}. \quad (2)$$

The two quantities depend only on the ratio κ of the cones' size. In the exact spherical case, when the line of sight is tracing a circle around the rotational pole, eq. (1) becomes modified: for a single value of Δ there exist two solutions for ρ_1, and two solutions for β (one positive and one negative, and of slightly different absolute value). However, numerical solution of the problem in spherical geometry suggests that for both values of β, eq. (2) remains intact (Fig. 5). Thus, in the spherical case β and ρ_1 scale in such a way that the simple eq. (2) is preserved, with no additional dependence on α or Δ involved. In what follows, eq. (2) will then be considered valid in general.

As can be seen in Fig. 4, in the nested cone model doubly fine-tuned conditions need to hold to generate the profile with equidistant components and deep central minimum. First, for a reasonable cone size ratio ($\kappa \gtrsim 0.5$) the impact angle β must be a precise fraction of ρ_1. Since β/ρ_1 changes very slowly with κ (for $\kappa \gtrsim 0.5$), even a small mistuning in β does not result in the equidistance. Second, to produce the equidistance, the line of sight must almost be grazing the very edge of the inner cone (Fig. 4). Wright (2003) has argued that both observational (Rankin 1993) and theoretical arguments support the value $\kappa = 0.74$, for which $\beta/\rho_1 = 0.95$. Thus, for the cone ratio typically found in statistical studies, the line of sight passes very close to the edge of the inner cone.[3] This implies that to observe the central minimum with the flux almost disappearing, the inner boundary of the inner cone (where the intensity almost vanishes) needs to be very close to the cone's peak, as marked in Fig. 4 with the thin quarter-circle arc. The location of this inner boundary needs to be extremely fine-tuned to reproduce the low flux at the centre of the profile.

Moreover, each inner-pair component has a roughly symmetric triangular shape, which would require a special, asymmetric emissivity profile of the inner cone, with the intensity dropping much faster on the inner side than on the outer side of the inner cone. Indeed, by matching the 1.5-GHz profile with Fig. 4, the inner half-thickness of the inner cone can be estimated to $(\delta\rho_1)_- \simeq \rho_1 - \beta = 0.05\rho_1$, whereas the the outer half-thickness of the inner cone is roughly equal to $(\delta\rho_1)_+ \simeq (\rho_2 - \rho_1)/2 = 0.17\rho_1$, which is considerably larger than $(\delta\rho_1)_-$.

The traditional nested-cone geometry can then be considered unacceptably fine tuned. The geometry invoked within the nested-cone model seems to be more contrived than we would expect based solely on the low statistics of such quadruple-and-symmetric profiles.

The situation does not much improve for a smaller cone ratio of $\kappa = 0.5$, because $\beta/\rho_1 = 0.79$ is still quite large in this case. The equidistancy condition implies that the smallest possible cone ratio is $\kappa = 1/3$, for which $\beta = 0$, *i.e.,* the line of sight is cutting through the cone centrally. However, this case is probably excluded by the limited slope of the polarisation angle curve. Therefore, the reasonable range of cone ratio for J0631+1036 can be limited to a quite narrow range: $\kappa \in (0.35, 0.5)$. We can basically say that for the nested cone model, the ratio between the angular radii of cones in J0631+1036 is around 0.4. This is much smaller than the typical value of 0.75. The value of β/ρ_1 is not tightly constrained, because the relation $\beta(\kappa)$ is steep around $\kappa = 0.4$ (see Fig. 5). The most likely value of β is somewhere between 0 and $0.7\rho_1$.

It is concluded that for the equidistant **conal** profile, the deep central minimum must result from either a very special cut through an extremely thin inner cone with a strange emissivity profile, or from a peculiar conal structure that has an uncommon cone size ratio. **An argument can be made that at least in this pulsar the beam is not circular but, say, oval, in a similar way as has been proposed to account for the apparent form of the precessing beams of B1913+16 and J0737–3039B (Weisberg & Taylor 2002; Carter & Weisberg 2008; Perera *et al.* 2010). However, introducing elongated *nested* cones with suitable axial ratios would amount to special pleading for such an essentially simple profile**. It would seem that an alternative to the classic double-cone model must be found for this pulsar.

IV. ALTERNATIVE EMISSION MODELS

Conal downflow models

In the hope of retaining a link to classic conal emission and radius-to-frequency mapping (RFM) we first examined whether any model can be found which sees some of the profile components of J0631+1036 as being generated by radiation from downflowing particles on the far side of the pulsar. Downflow has occasionally been discussed in other pulsars but as yet not convincingly (*e.g.,* in B1822–09, Dyks et al. 2005). Nevertheless, in the context here such a model would still be based on a conal radius-to-frequency mapping (RFM), a feature which seems to serve us reasonably well in many regular pulsars, and the symmetry of the model might naturally account for the most dramatic feature of J0631+1036: its near-symmetric profile.

In J0631+1036 an obvious step would be to assign two of its peaks to nearside emission and two to farside.

[3] By 'passing near the edge of the inner cone' we mean the passage which is nearly tangent to the mathematical cone corresponding to the *peak* flux of the inner components, not to be confused with the low-intensity boundary of the cone, discussed below.

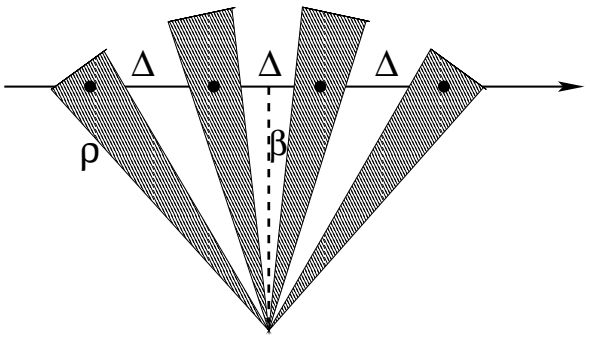

Figure 6. The wedge model: our line of sight cutting a fixed sequence of four similar wedge-shaped emission streams (the equivalent of Fig. 4 for the double cone model). This geometry naturally produces wider outer components and creates a central gap. Note that the observed peak intensity will not coincide with the geometric centre of the beam if there is an intensity gradient *along* the beam.

This can be done in two ways: either assign components 1 and 3 to a nearside cone (hence 2 and 4 from farside downward emission) or components 1 and 2 on the nearside (and 3 and 4 from the farside). Although these models led to not unreasonable emission heights, the generated PPA swings failed to yield SGs at the observed position on the far trailing side. The symmetric pattern of component thickness was also lost.

Finally, a further and more adventurous model was tried. We supposed that the outer components arise from identical single beams at either pole, each forming a narrow axisymmetric cone about the pulsar's magnetic axis. Then the outer components of J0631+1036 are the frequency-dependent manifestation of the upward nearside and downward farside emission at a particular height, and our sightline comes closest to the magnetic axes at this height at the component centres. It was assumed that the inner components may arise as caustic effects, so that intrinsically weak emission is boosted to detectable levels by the geometric coincidence of our line of sight moving instantaneously parallel to the trajectory of the emitting particles (see Dyks *et al.* 2010a).

This model did succeed in naturally identifying the fiducial point as a deep minimum (as observed) and yielded the correct sequence of component sizes at plausible heights, but required that the SG position was determined entirely by the nearside emission. This weakness, together with its unprecedented reliance on caustic emission, meant that the model failed to be convincing, but seems the best available if we are to retain both the conal hypothesis and RFM.

Wedge-shaped models

A second approach is to insist that the observed radio emission arises entirely on the nearside of the pulsar, but to abandon the assumption that the pulsar's emission has conal structure. Instead, we assume that the emission regions are arranged around the dipole axis in the form of fixed wedge-shaped segments (Fig. 6). In the case of J0631+1036, we must assume our line of sight traverses four distinct streams (or fans) of emission. The observed component sizes, and the separation between them, then depend on the time spent by the line of sight within each stream and not only on the wedges' intrinsic widths.

Interesting emission models of this kind have been developed in recent years (Dyks *et al.* 2010b (henceforth DRD10b), Wang *et al.* 2014, Dyks & Rudak 2014). These dispense with the need for RFM because its effects in conal geometry can be mimicked by azimuthal (ϕ) and co-latitude (θ) variations within the fan-shaped emission streams. In the last of the above references (Dyks & Rudak 2014) the authors are able in principle to reproduce the basic profile classes of ET VI (Rankin 1993), namely T, Q and M. Since in §2 we identify J0631+1036 as belonging to the statistically rare Q (four-component) class, it is of great interest to see how the new ideas can be applied to this very concrete example.

In the case of J0631+1036 the strongest constraint on models is the very clear, almost classic, PPA swing across the profile ending with a strong dip at the trailing edge. Within the range of possible wedge models, the lag can be attributed either, at one extreme, to the intrinsic, geometric asymmetry of the beam, or, at the other, to the corotational effects at a non-negligible emission altitude (BCW). In the former case, the PPA dip occurs at the neutron star's fiducial point, so that the trailing half of the profile is "missing" (Lyne & Manchester 1988, ET IX) and the components we see result from emission close to the surface (less than about 10 stellar radii). Alternatively, as with the conal model, we can assume the emission to be intrinsically symmetric about the fiducial point with the PPA dip shifted by standard A/R effects (BCW).

We have examined both cases in detail. In the first case the intrinsic emission pattern will inevitably be asymmetric, with the line of sight encountering no emission in the second half of the profile. We experimented with an intrinsic pattern of two broader outer beams separated by two narrower beams. and attempted to reproduce the apparent near-symmetry of the observed profile (noting that component 1 is observed to be significantly broader than component 4). Surprisingly, it proved impossible to find a consistent set of stream widths which would reproduce the observed profile, even when the assumed values of α and β were allowed to vary. This is essentially because the fan geometry demands that a stream on the leading edge will always appear wider than an identical stream at the meridian and the effect is always greater than that observed.

This model also lacks any obvious means of generalisation: the choice of wedges which are present/absent seems arbitrary, and indeed if the "full" profile were present it would seem that *eight* wedges could be detected in some pulsars, and this is never seen.

The alternative model shown in Fig. 6 is far more promising. Here all four streams are assumed intrinsically identical and there are no "empty" regions for the line of sight to traverse. The observed emission is assumed to

occur at the height ($\approx 600km$) suggested by the PPA swing, and the flat geometry implicitly assumes a large α. This model—with its perfect symmetry—serves well to illustrate the advantages of the wedge model in the context of J0631+1036:

1. The four components will be observed to have two broader outer and two narrow inner components.
2. The deep minimum at the centre of the profile can naturally be interpreted as the space between two streams (in contrast to the difficulties found with fine-tuning the double cone geometry in Fig. 4).
3. The approximate equidistance of components can have two possible explanations. Either the subbeams are themselves equidistant, but observed over a limited range of magnetic azimuth (i.e. are located near the main meridian), so that β is not much less than ρ (see Fig. 6). Alternatively, and more generally, the system may extend over the entire polar half-circle, but the azimuths of the inner and outer subbeams must be such that the central separation between the inner subbeams are significantly larger than that between the inner and outer ones.

The profile of J0631+1036 may therefore be so exceptional in the canon of pulsar profiles for one of two reasons: 1) it has a system of equidistant subbeams, but these are closer together than in most pulsars, or 2) most pulsars have unequally separated subbeams, but in this pulsar our line of sight traverse fulfils the equidistance condition.

4. Emission confined to a wedge shape can naturally produce the frequency-independent separations of components (no apparent RFM). This is easiest understood in the limit of infinitely narrow wedges. In such a case, components can only be observed when the line of sight is crossing the appropriate magnetic azimuth, regardless of frequency. However, a lack of RFM can also be expected for wide streams if their broad-band emission is spectrally uniform, i.e. when different parts of a given subbeam have a spectrum with the same shape but different normalisation. This is consistent with the weakness of RFM in J0631+1036 between 0.3 and 1.4 GHz defined by peak-to-peak separation (Figs. 2 and 3). Strong spatial RFM along each subbeam, (emission into narrow-band patches at increasing distance from the dipole axis), is unlikely in this pulsar (see Fig. 2 in Dyks & Rudak 2014).

Omitted from the above discussion are the small but significant asymmetries observed within the predominantly symmetric profile. These are (1) the leading component is slightly wider that the trailing component and (2) the centroid of the inner components is slightly shifted with respect to the centroid of the outer components. There are two possible reasons for this. First, the intrinsic alignment of the streams may not be perfectly symmetric about the meridian. In fact, it can be argued (Dyks & Rudak 2014; Wang *et al.* 2014) that this is not normally the case for most pulsars and thereby gives rise to apparent "core" components. Second, there may be differential A/R effects at the assumed emission altitude between the inner and outer components. Detailed discussion can be found in Dyks & Rudak (2014) (see their fig. 11).

A further interesting implication from the relative lack of profile asymmetries is that the observed radio emission of this pulsar originates from a narrow range of heights. Not only is there no evidence of increasing peak separation with lower frequency, but also the phase position of the SG does not display any measurable shift (§2). In a model with near-identical, equally separated subbeams, the beam system should not extend too far from the main meridian, which favours large β. Since the SG value ($R_{PA} = \sin\alpha/\sin\beta$) is reasonably well-determined (§2), a high β implies a high α. These values can be higher than those expected from the double cone model (§2)—and more consistent with the high α values independently deduced from the Fermi LAT pulsed γ-ray detections of this pulsar (Weltevrede *et al.* 2010, Seyffert *et al.* 2011). These studies suggest that α is at least 71°, depending on which (γ-ray) beam model is assumed.[4]

VII. SUMMARY AND DISCUSSION

Pulsar J0631+1036 presents a very interesting instance in which the core/double cone model of radio pulsar emission geometry has difficulty in giving an adequate description. The spectacular symmetric four peaks of its profile at 1.4 GHz immediately suggest a double cone structure, but careful application of the model fails to give the ratio of conal emission radii derived for most pulsars and implies that the (putative) inner and outer cones are emitted at the same physical height (§2). Such results have not been seen before in the pulsar population to which these ideas have been applied.

Under normal circumstances the apparent presence of a double cone would lead us to examine the pulsar's physics in terms of the classic Ruderman & Sutherland (1975) polar cap model or its more recent modifications (*e.g.,* Gil & Sendyk 2000). However, in the case of J0631+1036 we find that the required double-cone geometry needs to be so contrived as to be implausible (see §3). Invoking emission from a downflow from the farside of the pulsar (§4) resolves some of the geometric issues but at the price of becoming physically implausible. It has to be said that conal geometry fails us in this pulsar.

In an alternative approach, we examined the "wedge" or "fan" model recently developed by a number of authors (DRD10b, Wang *et al.* 2014, Dyks & Rudak 2014). This model explains pulsar profiles in terms of fixed streams of emission azimuthally arranged around the magnetic pole. Unlike the double cone picture, the model does not presuppose any specific polar cap physics, nor any prescribed frequency distribution within its streams, and this gives it great flexibility. It also differs in that it has little to say about single-pulse behaviour, an aspect we could not explore with our observations, since these revealed no organised modulations in any component.

In applying the model to J0631+1036 we tested two extreme versions. Firstly, we regarded the profile as arising from an intrinsically one-sided beam consisting of four emission lobes located ahead of the fiducial plane

[4] It must be remembered, however, that small β is allowed in models with unequal subbeam separations and widths.

close to the pulsar surface. This would then appear to have "missing" components on their trailing sides (Lyne & Manchester 1988, ET IX) and thereby explain why the PPA swing occurs so much later than the profile centroid. However, even allowing for differing thicknesses in the emission lobes and different impact angles (β), it proved impossible to generate the near-symmetric form of the pulsar's profile.

In a second, and more successful, version of the model we accepted that the shifted PPA swing was telling us that the profile was being produced at a specific height in the magnetosphere (about 600 km) and found that it could be closely modelled by our line of sight cutting across four fans of emission of similar intrinsic thickness and separation. However, this required the the beam system to be of limited azimuthal extent, implying a possible pulsar geometry with large impact angle β and inclination α. Given the difficulty of such estimates, a high inclination α seems to be compatible with the inferred values from radio (§2) and γ-ray studies (Weltevrede *et al.* 2010, Seyffert 2011).

It therefore seems that we have found a self-consistent picture for the production of this pulsar's profile. It supports a view that multi-peaked profiles result from random line of sight intersections across spokes of fixed emission wheels centred on the magnetic pole. In this view, "core" emission, found in many pulsars, is just another spoke of the wheel which we see with a different spectrum. So J0631+1036 owes its dramatic profile partly to chance alignment of the wheel, and partly to our highly oblique line of sight.

We conclude that J0631+1036 is yet another example of a pulsar with azimuthally-structured wedge-shaped streams of emission, and joins the group of objects, such as J0437−4715, for which the stream-like nature of its apparently conal components was unambiguously determined in DRD10b. Recent beam maps of precessing pulsars (J1906+0746, Desvignes et al. 2012; J1141–6545, Manchester et al. 2010) provide further examples of such objects, and confirm the predictions of DRD10b.

Thus the model has had some successes so far. However, we need to recognise that its high degree of flexibility, while giving it an advantage over the more rigid double-cone model, comes from the fact that it does not direct us – as yet – to any specific polar cap physics. As pointed out in Dyks & Rudak (2014), there needs to be a greater range of pulsars studied, and in single-pulse detail, before we can claim a proper understanding of pulsars.

Acknowledgments: The authors thank the many colleagues who responded to our challenge to consider the issues that pulsar J0631+1036 raises and have thus contributed to the discussions above. We also thank Dipanjan Mitra for adapting the RVM fitting software. GAEW thanks the Universities of Sussex and Manchester for Visiting Fellowships, and the Nederlandse Organisatie voor Wetenschappelijk Onderzoek (NWO) for a Visitor Bursary held at the "Anton Pannekoek" Astronomy Institute (API) of the University of Amsterdam. JMR also thanks the NWO for for a Visitor Grant and the API for their hospitality. Portions of this work were carried out with support from US National Science Foundation (NSF) Grant AST 08-07691. Another part was supported by Polish National Science Centre grant DEC-2011/02/A/ST9/00256. Arecibo Observatory is operated by SRI International under a cooperative agreement with the US NSF, in alliance with Ana G. Mndez-Universidad Metropolitana, and the Universities Space Research Association. This work used NASA ADS system.

REFERENCES

Blaskiewicz, M., Cordes, & J.M, Wasserman, I, 1991, *Ap.J.*, 370, 643 (BCW)
Clifton, T., & Weisberg, J. M., 2008, *Ap.J.*, 679, 687
Desvignes, G., Kramer, M., Cognard, I., Kasian, L., van Leeuwen, J., Stairs, I., Theureau G. 2012, Proc. IAU Symposium No. 291, ed. J. van Leeuwen, 199
Dyks, J., Rudak, B., & Harding, A. K. 2004, *Ap.J.*, 607, 939
Dyks J., & Rudak B., 2014, MNRAS, submitted
Dyks, J., Zhang, B., & Gil, J. 2005, *Ap.J.*, 626, 45
Dyks, J., Wright, G.A.E., & Demorest, P., 2010a, *MNRAS*, 405, 509
Dyks, J., Rudak, B., Demorest, P. 2010b, *MNRAS*, 401, 1781 (DRD10b)
Espinoza, C. M., Lyne, A. G., Stappers, B. W., & Kramer, M. 2011, *MNRAS*, 414, 1679
Force, M. M., & Rankin, J. M. 2010, *MNRAS*, 406, 237
Gangadhara R. T., & Gupta Y. 2001, *Ap.J.*, 555, 31 (G&G)
Gil, J., Sendyk, M., 2000, *Ap.J.*, 541, 351
Lyne, A. G., & Manchester, R.N., 1988, *MNRAS*, 234, 477
Malov, I. F., & Suleymanova, S.A. 1998, *Astron. Rep.*, 42, 388
Manchester, R.N. *et al.* 2010, *Ap.J.*, 710, 1694
Mitra, D., Rankin, J. M. 2010, *Ap.J.*, 727, 92 (ET IX)
Mitra, D., Arjunwadkar, M. & Rankin, J. M. 2014, *Ap.J.*, submitted (ET X)
Perera, B.B.P., McLaughlin, M. A., Kramer, M., Stairs, I. H., Ferdman, R. D., Freire, P.C.C., Possenti, A., & Breton, R. P., *et al.* 2010, *Ap.J.*, 721, 1193
Rankin, J. M. 1983, *Ap.J.*, 274, 333 (ET I)
Rankin, J.M. 1993, *Ap.J.*, 405, 285 and *A&A Suppl.*, 85, 145 (ET VI)
Ruderman, M., & Sutherland, P., 1975, *Ap.J.*, 196, 51
Seyffert, A. S., Venter, C., de Jager, O. C., & Harding, A. K. 2011, arXiv:1105.4094v1
Smith, E., Rankin, J., & Mitra, D. 2013, *MNRAS*, 435, 1984
Srostlik, Z., & Rankin, J. M. 2005, *MNRAS*, 362, 1121
2010, *MNRAS*, 406, 1029
Wang, H.G. *et al.* 2014, *Ap.J.*, 789, 1
Weisberg, J. M., & Taylor, J. H., 2002, *Ap.J.*, 576, 942
Weltevrede, P., *et al.* 2010, *Ap.J.*, 708, 1426
Weltevrede P., Abdo A. A., Ackerman M., Ajello M., Axelsson M., Baldini, L., *et al.* 2010, *Ap.J.*, 708, 1426
Wright, G. A. E., 2003, *MNRAS*, 344, 1041
Yuan, J. P., Wang, N., Manchester, R. N. & Liu, Z. Y., 2010. *MNRAS*, 404, 289.
Zepka, A., Cordes, J. M., & Wasserman, I., Lundgren, S. C. 1996, *Ap.J.*, 456, 305